High-throughput Nano-DESI Mass Spectrometry Imaging of Biological Tissues Using an Integrated Microfluidic Probe

Xiangtang Li[a], Hang Hu[a], Ruichuan Yin[a], Yingju Li[b], Xiaofei Sun[b], Sudhansu K. Dey[b], and Julia Laskin[a]*.

[a]Department of Chemistry, Purdue University, West Lafayette, IN 47907, United States

[b]Division of Reproductive Sciences, Cincinnati Children's Hospital Medical Centre and Department of Pediatrics, University of Cincinnati College of Medicine, Cincinnati, Ohio, 45229, United States

ABSTRACT: Nanospray desorption electrospray mass spectrometry imaging (nano-DESI MSI) enables quantitative imaging of hundreds of molecules in biological samples with minimal sample pretreatment and a spatial resolution down to 10 μm. We have recently developed an integrated glass microfluidic probe (iMFP) for nano-DESI MSI, which simplifies the experimental setup and enables imaging with a spatial resolution of 25 μm. Herein, we describe an improved design of the iMFP for the high-throughput imaging of tissue sections. We increased the dimensions of the primary and spray channels and optimized the spray voltage and solvent flow rate to obtain a stable operation of the iMFP at both low (0.04 mm/s) and high (0.4 mm/s) scan rates. We demonstrate the performance of the high-throughput iMFP by imaging mouse uterine and brain tissue sections. We observe that the sensitivity, molecular coverage, and spatial resolution obtained using the iMFP do not change to a significant extent as the scan rate increases. Using a scan rate of 0.4 mm/s, we obtained high-quality images of mouse uterine tissue sections (scan area: 3.2 mm×2.3 mm) in only 9.5 minutes and of mouse brain tissue (scan area: 7.0 mm×5.4 mm) in 21.7 minutes, which corresponds to a 10-15-fold improvement in the experimental throughput. We have also developed a quantitative metric for evaluating the quality of ion images obtained at different scan rates. Specifically, by defining regions of interest (ROI) in both a representative ion image and optical image of the tissue section, we calculated the spatial deviation between the two ROIs by counting the number of mismatched pixels. Using this metric, we demonstrate that the percent deviation increases slightly from 6.7% to 10.2 % with an increase in the scan rate from 0.02 to 0.4 mm/s. The maximum experimental throughput achieved in this study is limited by the acquisition rate of a mass spectrometer necessary to achieve the desired spatial resolution and may be further improved using a faster instrument. The ability to image biological tissues with high throughput using iMFP-based nano-DESI MSI will substantially speed up tissue mapping efforts.

Mass spectrometry imaging (MSI)[1-8] is a powerful tool for the label-free mapping of the spatial distributions of hundreds of biomolecules in biological samples in a single experiment. Ambient ionization techniques[5-7, 9, 10] are growing in their popularity in MSI due to their ability to provide molecular maps of biological samples in their native state. Liquid extraction-based ambient ionization techniques are of particular interest to this work.[6, 11] These include desorption electrospray ionization (DESI),[12-14] nanospray desorption electrospray ionization (nano-DESI),[9, 15-17] liquid microjunction surface sampling probe (LMJ-SSP),[18, 19] and liquid extraction surface analysis (LESA).[20, 21] Although typically ambient MSI experiments are performed with a spatial resolution of 50-150 μm, tissue imaging with a spatial resolution of better than 10 μm has been achieved using nano-DESI and single probe MSI.[10, 16, 22] Recent developments have been focused on imaging and identification of proteins and protein complexes in biological tissues along with multimodal imaging which substantially broadens the range of applications of these techniques.[23-26]

The experimental throughput is one of the key challenges in high-resolution MSI experiments. Indeed, the number of pixels and the total acquisition time increases quadratically with increase in the spatial resolution. Therefore, it is essential to develop high throughput acquisition methods for MSI. Several studies have reported high-throughput MSI using matrix-assisted laser desorption ionization (MALDI).[27-31] For example,

a continuous laser raster sampling in the typewriter mode was implemented on a commercial MALDI-TOF instrument and used for imaging of a rat brain tissue section with a total area of 185 mm² at a spatial resolution of 100 µm in approximately 10 min.[32] In another study, a Nd:YLF solid-state laser with pulse repetition rates up to 5 kHz was coupled to a MALDI TOF/TOF instrument.[33] The system was operated in a continuous laser raster mode with high acquisition rates of 50 pixels/s to acquire MSI data with a spatial resolution of 100 µm. Collectively, these developments provided an 8-14 times improvement in the experimental throughput in comparison with conventional TOF/TOF and ion trap systems.[33] Recently, a transmission geometry MALDI ion source has been used for imaging of proteins in tissues using a laser spot diameter of 1 µm and a raster step size of 2.5 µm. Using a continuous laser raster mode and an acquisition rate of 40 pixels/s, that study demonstrated protein imaging with high throughput and a subcellular spatial resolution.[28]

High throughput approaches have also been developed for ambient imaging using DESI and nano-DESI. Because the experiments are performed by continuously scanning the sample in lines and stepping between the lines, the scan rate of the sample stage is the key parameter that determines the total acquisition time. The stability of the sampling and ionization may be affected by the scan rate and are typically re-optimized to enable high throughput analysis. A stable DESI sprayer has been designed and coupled to a fast-scanning quadrupole time-of-flight mass spectrometer to improve the throughput and stability of DESI-MSI.[34] The overall acquisition time for imaging of a 10 mm × 10 mm rat brain tissue sample with a spatial resolution of 60 µm was ~1 hour.

In nano-DESI-MSI, a liquid bridge formed between two capillaries is used for the localized liquid extraction from the sample.[10, 35] The extracted analytes are transferred through a short nanospray capillary to a mass spectrometer inlet and ionized by electrospray ionization. The throughput of nano-DESI MSI experiments is limited by the stability of the liquid bridge and the transfer time of the analytes through the nanospray capillary. We have previously used high-speed acquisition with a scan rate of 0.2 mm/s to generate 3D images of mouse uterine tissue.[36] In that study, multiple tissue sections were arranged on the same glass slide and imaging was performed over an area of 20 mm ×16 mm with a spatial resolution of 150 µm and an acquisition rate of 5 Hz. The total scan time was 4.5 hrs and the scan rate was limited predominately by the transfer time through the nanospray capillary and the relatively low acquisition rate of the mass spectrometer. Meanwhile, the stability of the liquid bridge was not critical in that study due to its relatively large size of 150 µm.

In contrast, nano-DESI imaging with a higher spatial resolution imposes more stringent constraints on the stability of the liquid bridge and requires a precise control of the distance between the nano-DESI probe and sample surface. We have previously developed two approaches for the constant distance mode nano-DESI MSI.[15, 37] The simplest approach involves a three-point-plane calibration of the tilt of the glass slide containing the sample, which is well-suited for flat samples.[15] In another approach, we use a shear force feedback to control the distance between the sample and nano-DESI probe, which enables imaging of samples with complex topography and high-resolution imaging of tissues sections.[10, 37]

Herein, we describe the design of a high-throughput integrated microfluidic probe (iMFP) for nano-DESI MSI. Previously, we have demonstrated that the iMFP provides a stable liquid bridge to the sample and enables imaging with a spatial resolution of 25 µm.[38] The iMFP shown schematically in **Figure 1A** contains two microfluidic channels that transfer the working solvent to and from the sample and a finely polished tip for ionization. In this work, we have optimized the design of the iMFP for the high throughput MSI experiments. This involved increasing the diameter of the channels to reduce the resistance of the solvent flow through the spray channel to a mass spectrometer. In addition, we optimized the sampling port configuration to improve the stability of the liquid bridge generated by the iMFP. We demonstrate a 10-15-fold improvement in the experimental throughput at a minimal loss to the quality of the imaging data.
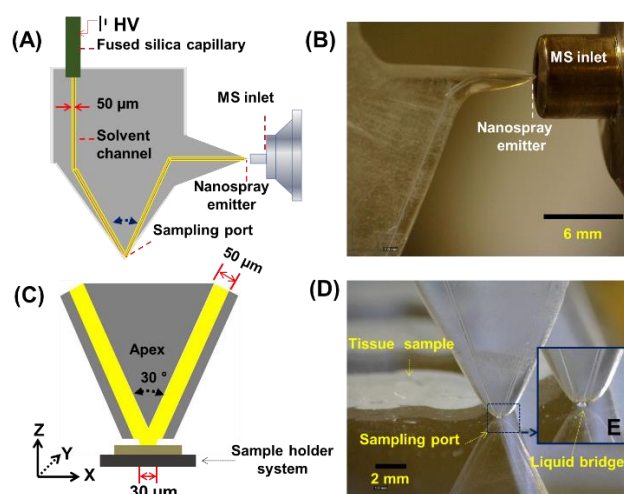

Figure 1. Design of the iMFP for high-throughput nano-DESI MSI: (A) A schematic diagram of the iMFP; (B) A photograph of the nanospray emitter approaching the inlet of a mass spectrometer; (C) A schematic illustration of the sampling port and liquid bridge; (D) A photograph of the sampling port touching a glass surface near the tissue sample; (E) An enlarged photo of the liquid bridge.

EXPERIMENTAL SECTION

Chemicals and Solvent Preparation.

LC-MS grade methanol (MeOH) and Omnisolv LC-MS grade water were purchased from MilliporeSigma (Burlington, MA). Lysophosphatidylcholine 19:0 (LPC 19:0) was purchased from Avanti Polar Lipids (Alabaster, AL). The extraction solvent in this study was composed of a 9:1 MeOH-water mixture containing 1 µM LPC 19:0 as an internal standard.

Biological Tissues.

Biological tissue sections were prepared according to our previously described procedures.[10, 17, 22, 38] Briefly, one uterine horn was collected from a mouse on day 4 of pregnancy, frozen in freezing media (Super Friendly Freeze`It™, Fisher), sliced to a series of sections with a thickness of 12 µm using a Leica CM 3050 cryostat, thaw-mounted onto pre-cleaned polylysine coated microscope glass slides, and stored at –80 °C. The mice were housed in the Cincinnati Children's Hospital Medical Center. Animals were housed in the animal care facility at the Cincinnati Children's Hospital Medical Center (CCHMC) using protocols approved by the Cincinnati Children's Hospital Research Foundation Institutional Animal Care and Use Committee. Mouse brain tissue sections from 10-week-old C57BL/6 mice were provided by Dr. Jordan Smith from PNNL and stored at –80 °C.

Fabrication of the high throughput iMFP.

The fabrication of the iMFP involves two main steps: First, a microfluidic chip with channel dimensions of ~50 µm×35 µm is fabricated by conventional photolithography, wet etching, and high-temperature bonding technique. The fabrication process of a glass microfluidic chip is described in our previous publication[38] and earlier reports.[39, 40] Brifely, a photomask with a channel size of 15 µm is first fabricated. The pattern of the channel structure is photocopied onto a chrome plate after UV exposure using a mask aligner system, and the chrome plate is subsequently developed and wet etched to form a substrate wafer with a channel dimension of ~50 µm × 35 µm by controlling the etchant concentration and time. After removing the photoresist and chromium layer, the substrate wafer is bonded with another blank glass wafer at 590° C for 3 hours to form the microfluidic chip. Second, the iMPF with a sampling port and a nanospray emitter is fabricated by a multistep grinding and polishing using a power tool and sandpaper. Next, a fused silica capillary (ID 50 µm, OD 150 µm) is connected to the solvent channel of the iMFP and sealed with epoxy. Before the probe is used for the first time, the sampling port, solvent channel, and spray channel are treated with a 5:1:1 (v/v/v) H_2O/HCl/H_2O_2 solution for 5 min. Prior to each imaging experiment, the channels and sampling port are washed with deionized water, 0.1 M HCl, 0.1 M NaOH, and again with deionized water for 5 minutes by vacuum suction.

The iMFP-Based Nano-DESI Imaging Platform.

The nano-DESI MSI platform is comprised of a syringe pump with a 2.5 mL syringe for solvent delivery, a micropositioner for the iMFP, XYZ motorized stages, a sample holder, and two Dino-Lite digital microscopes for monitoring the nano-DESI probe during imaging experiments.[22] One of the microscopes is focused on the sampling port and another one monitors the nanospray emitter tip and MS inlet. The iMFP is mounted onto a micropositioner and positioned in front of a mass spectrometer inlet. The distance between the nanospray emitter tip and the MS inlet orifice is ~0.5 mm. A 10 cm long fused-silica capillary of 50 µm inner and 150 µm outer diameter (Molex, Thief River Falls, MN) connected to a syringe pump supplies the solvent to the iMFP. The spray voltage of +3.2 kV is applied to the syringe needle through a high-voltage cable. A 10-MΩ resistor is integrated into the high-voltage cable to avoid potential electric shock induced by a high spray voltage. A microscope glass slide containing tissue sections is mounted onto the sample holder. The XYZ stage used for sample positioning is controlled by a custom LabVIEW program. The extraction solvent is propelled through the iMFP to the sampling port, which is positioned to form a stable liquid bridge to the sample surface; the extracted analyte molecules are delivered to the mass spectrometer through the spray channel.

Mass Spectrometry Imaging Experiments.

Nano-DESI MSI experiments were performed using a Q-Exactive HF-X mass spectrometer. A high voltage of +3.2 kV and an RF Funnel voltage of +100 V were applied in positive mode; the heated capillary was held at 250 °C. Mass spectra were acquired in the range of m/z 133–2000 with a mass resolution of 60,000 at m/z 200. The AGC target was 1×10^6 and the maximum injection time was 200 ms. MSI data were acquired in lines by scanning the sample under the iMFP using a motorized XYZ stage (Zaber, Technologies, Vancouver, BC) and stepping between the lines. The distance between the iMFP and sample was controlled using the "three-point plane" method.[41] This method automatically compensates for the tilt of the sample surface by defining the coordinates of three points outside of the tissue section by landing the nano-DESI probe on the glass surface. Imaging experiments of mouse brain tissue sections were performed using scan rates of 0.04 mm/s, 0.2 mm/s and 0.4 mm/s and the step between the lines of 78 µm. For imaging of mouse uterine tissue sections, we used the first generation iMFP to generate ion images at the scan rates of 0.02 mm/s and 0.04 mm/s and 30 µm spacing between the lines. Meanwhile, the newly designed high-throughput iMFP was used to acquire data at scan rates of 0.15mm/s, 0.2 mm/s, 0.25 mm/s, and 0.4 mm/s with a 40 µm spacing between the lines.

Data Analysis.

Each line scan was acquired as an individual RAW file using Xcalibur software (Thermo Electron, Bremen, Germany). A custom-designed Python code (https://github.com/LabLaskin/MSI-image-generator) was used to visualize ion images. RAW files were processed using pyMSfilereader. Ion signals of each selected m/z feature were extracted from mass spectra using a mass tolerance window of ±10 ppm, normalized to the total ion current (TIC), and aligned with respect to sampling locations. To evaluate the data quality of the high-throughput iMFP experiments at different scan rates, regions of interest (ROIs) were extracted from ion images of a tissue section and compared with the corresponding ROIs in the optical image. First, a selected ion image was automatically registered to an optical image with affine transformation using elastix (https://github.com/InsightSoftwareConsortium/ITKElastix). Second, ROIs from both modalities were generated by multi-Otsu thresholding approach following our previous report.[42] Finally, both ROIs were superimposed to calculate percent deviation of ROI areas using an optical image as a reference to evaluate the MSI data quality.

The identification of phospholipids and metabolites observed in imaging experiments was performed based on the accurate mass measurement and MS/MS data obtained directly on a tissue section.

RESULTS AND DISCUSSION

The stability of the liquid bridge and rapid transfer of the extracted analytes to a mass spectrometer are critical factors

that determine the quality of the high throughput nano-DESI MSI experiments. Specifically, the stability of the liquid bridge affects both the signal stability and quantitative capabilities of nano-DESI MSI, which require that the volume of the liquid bridge remains constant throughout the experiment. Meanwhile, the rate of analyte transfer to a mass spectrometer determines the correspondence between the location of analyte extraction and observed signal. Slow analyte transfer results in signal tailing, which is detrimental to the spatial resolution and quality of nano-DESI MSI data.

We have re-designed the iMFP in order to meet these criteria. Specifically, we have fabricated the iMFP shown in **Figure 1A** with a channel size of 50 μm × 35 μm as compared to 40 μm × 25 μm channels used in the previous design.[38] As the channel size increases, the solvent flow rate also increases, which ensures faster transfer of analytes through the iMFP. **Figure 1B** shows a photograph of the nanospray emitter positioned in front of the mass spectrometer inlet. The size of the liquid bridge is controlled by the solvent flow rate, the distance between the sampling port and sample surface, and the distance between the nanospray emitter and inlet, which determines the rate of vacuum-assisted solvent transfer through the spray channel. We found that using wider channels, we could still maintain a stable liquid bridge of ~30 μm in diameter on the sample surface by optimizing these parameters. The configuration of the sampling port shown in **Figure 1C** was optimized for the high throughput experiments. The angle between the channels is 30⁰ and the apex of the iMFP is located ~20 μm above the edge of the device. **Figure 1D** shows a photograph of the liquid bridge on the glass surface. A small and stable liquid bridge was obtained by optimizing several experimental parameters including the distance between the iMFP and the inlet, high voltage, distance between the sampling port and surface, and solvent flow rate.

The distance between the nanospray emitter tip and instrument inlet affects both the stability of the spray and magnitude of the signal. We found that the optimal distance was ~0.5 mm. For this distance, the optimized high voltage that provides the most stable signal and highest signal-to-noise ratio is in the range of 3 -3.5 kV as shown in **Figure S1** of the supporting information (SI). The high throughput nano-DESI MSI experiments described in this study were performed using the high voltage of 3.2 kV.

The flow rate of the extraction solvent determines the stability of both the liquid bridge and electrospray. When the flow rate is low, the size of the liquid bridge is too small and it readily loses contact with the sample when the sample stage is running at a high speed. In contrast, when the flow rate is too high, the spray channel becomes a bottleneck for the solvent transfer through the iMFP, which results in an uncontrolled accumulation of the solvent at the sampling port. Therefore, the optimization of the solvent flow rate is critical to obtaining a stable performance of the high-throughput nano-DESI MSI experiments. To examine the effect of the solvent flow rate on image quality, we conducted several experiments at a scan rate of 0.4 mm/s. Line scans obtained for phosphatidylcholine, PC 34:1, at different flow rates are shown in **Figure S2**. We observed an unstable signal and low-quality ion images at a flow rate of 1.1 μL/min, which is attributed to the intermittent disruption of the contact between the liquid bridge and sample surface. Stable ion signals and high-quality MSI data were obtained at a flow rate of 1.5 μL/min. However, further

increase in the flow rate to 1.7 μL/min resulted in a substantial increase in the size of the liquid bridge and signal tailing as shown in **Figure S2D.**

All subsequent high throughput MSI experiments were performed using the "three-point plane" mode described earlier, a high voltage of 3.2 kV, flow rate of 1.5 μL/min, and scan rate of 0.4 mm/s. At lower scan rates, the flow rate was reduced to ensure the stability of the liquid bridge. For example, flow rates of 1.1 and 1.3 μL/min were used for imaging at scan rates of 0.04 and 0.2 mm/s, respectively.

Figure 2 shows a comparison of the imaging data obtained for mouse brain tissue sections at different scan rates ranging from 0.04 mm/s to 0.4 mm/s using the same iMFP. We compared the signal stability, sensitivity, image quality, spatial resolution, and image acquisition throughput. Line profiles obtained for PC 34:1 (m/z 782.558) from a similar region of a mouse brain tissue section at scan rates of 0.04 mm/s, 0.2 mm/s, and 0.4 mm/s are shown in **Figure 2A**. Aside from the smoothing effect that increases with decrease in the number of pixels, we observe a similar signal stability at different scan rates indicating a stable operation of the iMFP at both low and high scan rates. Both the line profiles in **Figure 2A** and representative single-pixel mass spectra in **Figure 2B** show comparable signal intensities at different scan rates indicating that the sensitivity of imaging experiments does not degrade with an increase in the scan rate.
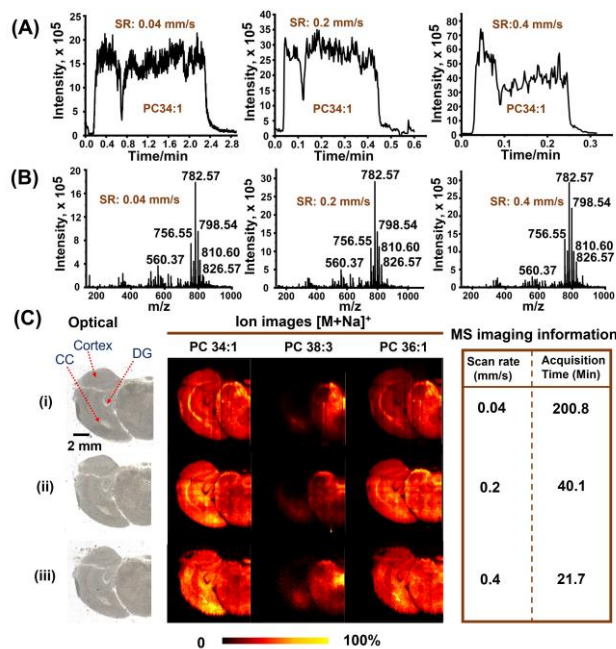

Figure 2. Imaging of mouse brain tissue sections at different scan rates of 0.04 mm/s, 0.2 mm/s, and 0.4 mm/s. (A) Representative line profiles of PC 34:1 (m/z 782.568) across a tissue section at different scan rates. (B) Single-pixel mass spectra obtained at different scan rates. (C) Optical images of tissue sections used at (i) 0.04 mm/s, (ii) 0.2 mm/s, and (iii) 0.4 mm/s scan rates. Representative positive mode ion images obtained for [M+Na]+ ions of PC 34:1 (m/z 782.568), PC 38:3 (m/z 834.599), and PC 36:1 (m/z 810.599) along with image acquisition times. The following regions are labeled in the optical image: cortex, dentate gyrus (DG), and corpus callosum (CC). Scale bar: 2 mm. The intensity scale: black (low), yellow

(high). Additional experimental parameters are listed in Table S1.

Representative ion images of mouse brain tissue sections obtained at different scan rates are compared in **Figure 2C**; the corresponding optical images are shown in the left column. We found that imaging with both low (0.04 mm/s) and high (0.2 mm/s and 0.4 mm/s) scan rates provides consistent spatial localization patterns of the three species, PC 34:1, PC 38:3, and PC 36:1, shown in the figure. Specifically, we observed a substantial enhancement of PC 34:1 and a slight signal enhancement of PC 36:1 in the corpus callosum (CC) region of the tissue. Meanwhile, both PC species are substantially suppressed in dentate gyrus (DG). Many MSI studies have reported that phospholipids from the same class but different acyl chain lengths and number of double bonds may show completely different localization in tissues. In the example shown in **Figure 2C**, PC 34:1 is observed in all regions of the brain tissue, but is somewhat enhanced in the cortex and substantially enhanced in the white matter region. In contrast, PC 38:3 is only localized to the brain stem region. These results illustrate that lipid composition has a pronounced effect on their localization, which may be attributed to differences in their biological function. Some differences in the distributions of phospholipids observed at different scan rates may be attributed to the fact that different coronal tissue sections were used in these experiments.

Despite the smaller number of pixels in ion images obtained at high scan rates, they provide a high-quality representation of the spatial localization of molecules in the sample. We do not observe any signal tailing, which indicates that the analyte transfer through the spray channel is sufficiently fast even at the highest scan rate. Meanwhile, the total acquisition time is reduced by almost a factor of 10, from 200.8 min at a scan rate of 0.04 mm/s to only 21.7 min at a scan rate of 0.4 mm/s.
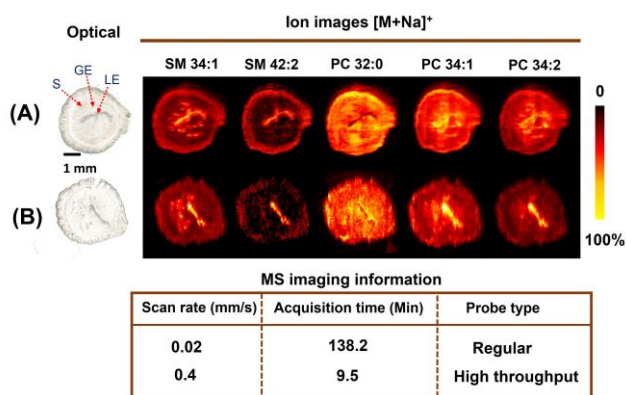

Figure 3. Imaging of mouse uterine tissue sections acquired at scan rates of (A) 0.02 mm/s and (B) 0.4 mm/s using a regular iMFP and high-throughput iMFP, respectively. Representative positive mode images of [M+Na]+ ions of PC 32:0 (m/z 756.552), PC 34:1 (m/z 782.568), PC 34:2 (m/z 766.575), SM 34:1 (m/z 725.557), and SM 42:2 (m/z 835.666). Ion images are normalized to TIC. Scale bar: 2 mm; the intensity scale: black (low), yellow (high). Image acquisition parameters are listed in Table S2.

To further demonstrate the performance of the high throughput iMFP, we have acquired high-quality ion images for smaller area mouse uterine tissue sections. In these experiments, we compared the results obtained using the regular iMFP at lower scan rates (**Figure 3A**) with the results obtained using the high throughput iMFP at high scan rates (**Figure 3B**). **Figure S3**, **Figure S4** and **Table S2** provide more detailed comparative analysis of line profiles, representative ion images, and image acquisition times for these samples. Mouse uterine tissue contains multiple cell types that generate distinct chemical gradients over a small area of ∼2 ×2 mm^2 making it an excellent model system for evaluating the performance of high-resolution imaging approaches.[22] We label the luminal epithelium (LE), glandular epithelium (GE), and stroma (S) in the optical image in **Figure 3A**. Representative positive images of [M+Na]+ ions of endogenous phospholipids (SM 34:1, and SM 42:2, PC 32:0, PC 34:1, PC 34:2,) in mouse uterine tissue sections obtained at scan rates of 0.02 mm/s and 0.4 mm/s are shown in **Figures 3A** and **3B**, respectively. We note that the scan rate of 0.02 mm/s is commonly used for high-resolution imaging of this type of tissue.[10, 22] The acquisition time per line scan is 130 s and 9 s for the scan rates of 0.02 mm/s and 0.4mm/s, respectively. Remarkably, we obtained similar-quality ion images even for this small sample. The observed molecular localizations are consistent with previous reports.[22, 38, 42] In particular, we observe the enhanced abundance of SM 34:1 in both LE and GE cells. Meanwhile, SM 42:2 and PC 34:2 are significantly enhanced only in LE cells and PC32:0 is suppressed in the LE region. The total acquisition time of only 9.5 min was achieved for this small sample using the high-throughput iMFP at a scan rate of 0.4 mm/s.
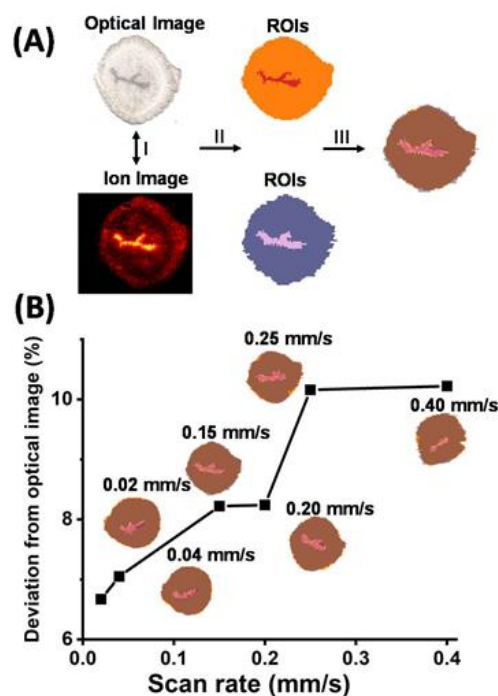

Figure 4. A spatial deviation analysis of ROIs from optical images and ion images to evaluate the data quality of MSI experiments at each scan rate. (A) A workflow to generate and

compare ROIs from optical images and ion images. (B) A plot of percent deviation of a representative ion image of SM 42:2 from the optical image at each scan rate. Process I: Spatial registration between optical image and ion image. Process II: ROIs are extracted separately using image segmentation. Process III: 2 ROI images are overlapped to calculate the percent deviation.

We have also estimated the spatial resolution of both the regular and high throughput iMFP devices. In nano-DESI MSI, the spatial resolution is usually evaluated using the "20% : 80% rule".[43] According to this rule, the spatial resolution is given by the distance over which the signals of the steepest features in the image change from 20% to 80% of the maximum signal span. Using this approach, we estimate that we achieved the spatial resolution of 25 μm at low scan rates. However, this approach fails as the number of points along the line profile decreases at higher scan rates. To address this problem, we have developed an image spatial deviation analysis method to evaluate the spatial resolution of ion images acquired at high scan rates.

Specifically, we have developed an image registration and segmentation-based workflow to evaluate the data quality of MSI experiments at different scan rates. SM 42:2 [M+Na]+ is localized to the LE region and tissue edge, which represents the spatial information that MSI is able to characterize. The same spatial feature is also characterized by a tissue scanner with higher resolution. We extracted and compared regions of interest (ROIs) from both modalities. This analysis enables a quantitative evaluation of the quality of high-throughput MSI data using an optical image of the tissue as a ground truth. **Figure 4A** outlines the workflow. In process I, the optical image and ion image of SM 42:2 are automatically co-registered using the affine transformation and stochastic optimization.[44, 45] In process II, image segmentation is performed separately for both images to create ROIs. The optical image with three RGB channels is segmented using the Gaussian Mixture Model clustering algorithm. Meanwhile, the Grayscale ion image is segmented using Multi-Otsu thresholding algorithm. Generation of ROIs using image segmentation was performed as described in a previous report.[42] Ion images and optical images have distinct frequencies, such that their spatial information cannot be directly compared. In ROI images, we assign discrete labels to pixels in both modalities, such that the spatial features can be compared using a unified labeling. Finally, in process III, ROIs, which represent LE and tissue edge features, are overlapped to evaluate the spatial deviation. Hamming distance, which represents counts of mismatched pixels in two ROIs, is computed and percent deviation of the ion image with respect to optical image is calculated using the optical image ROIs as ground truth. The equations for Hamming distance and percent deviation are provided in Eq(1) and Eq(2), respectively.

$$d(I,O) = \sum_{j=1}^{k} I[j] \oplus O[j] \qquad (1)$$

$$Percent\ deviation = \frac{d(I,O)}{\sum_{i=1}^{k} O[i] \oplus 0} \times 100\% \qquad (2)$$

where, I and O are ROI images from ion image and optical image with k total pixels. Pixels at off-tissue, LE and other tissue regions are labeled as 0, 1 and 2 in ROI images, respectively. ⊕ denotes an exclusive disjunction operator. Overlapped ROIs and percent deviations calculated for ion images acquired at six scan rates are summarized in **Figure 4B**. Percent deviation increases slightly with increase in the scan rate. For example, the ion image acquired at 0.02 mm/s has the smallest percent deviation (6.7%). Meanwhile, percent deviation obtained for ion images acquired using scan rates of 0.25 mm/s and 0.4 mm/s is 10.16% and 10.22%, respectively. The increase in percent deviation is mainly attributed to broadening of the signal in the LE region and loss of the ion signal at tissue edges. Despite the observed increase in percent deviation of ion images at high scan rates, the values of ~10% obtained at high scan rates is still quite low, which confirms that the substantial increase in the experimental throughput obtained using the high-throughput iMFP device comes at a little expense to the quality of chemical imaging data. Raw images and ROIs for MSI experiments at six scan rates are available in **Figure S5**.

CONCLUSION

We have developed a high-throughput iMFP for molecular imaging of tissue samples using nano-DESI MSI and demonstrated a 10-15-fold increase in the experimental throughput with little or no loss of the quality. We have also introduced a quantitative metric for evaluating the quality of the high throughput MSI data by calculating the percent deviation of the ion image from the optical image. We demonstrate that high throughput MSI using a specially-designed iMFP retains the sensitivity, signal stability, image quality, and spatial resolution obtained at lower scan rates. This indicates that the iMFP forms a stable liquid bridge on the sample surface at high scan rates and a spatial resolution of 25 μm, which imposes stringent requirements on the stability of the probe during image acquisition. The acquisition time of <10 min per image was achieved for smaller mouse uterine tissue sections and <22 min for larger mouse brain tissue sections.

Further improvement in the experimental throughput of the iMFP may be achieved by (1) shortening the length of the spray channel; (2) installing the shear force probe to control the distance between the sampling port and sample surface,[10] and (3) developing a new sampling port geometry suitable for scanning the probe with higher scan rates. We note that the spatial resolution of the high throughput iMFP is limited by the acquisition rate of a mass spectrometer. Coupling the high throughput iMFP with a faster mass spectrometer is necessary imaging with high spatial resolution. The development reported herein will substantially enhance tissue mapping efforts and facilitate 3D imaging of biological tissues.

Supporting Information

The Supporting Information is available free of charge on the ACS Publications website.

AUTHOR INFORMATION

Corresponding Author

* Prof. Julia Laskin
Department of Chemistry, Purdue University
560 Oval Drive, West Lafayette, IN 47907 (USA)
E-mail: jlaskin@purdue.edu
TEL: 765-494-5464.

Safety Considerations

A high spray voltage of +3.2 kV is applied to the syringe needle for ionization. The users must switch the instrument to the standby mode before touching the crocodile clip of the high voltage cable.

Notes

The authors have no conflict of interest to declare.

ACKNOWLEDGMENTS

REFERENCES

1. Stoeckli, M.; Chaurand, P.; Hallahan, D. E.; Caprioli, R. M., Imaging mass spectrometry: a new technology for the analysis of protein expression in mammalian tissues. Nat. Med. 2001, 7, 493-496.
2. Buchberger, A. R.; DeLaney, K.; Johnson, J.; Li, L., Mass spectrometry imaging: a review of emerging advancements and future insights. Anal. Chem. 2018, 90, 240.
3. McDonnell, L. A.; Heeren, R. M., Imaging mass spectrometry. Mass Spectrom. Rev. 2007, 26, 606-643.
4. Norris, J. L.; Caprioli, R. M., Analysis of tissue specimens by matrix-assisted laser desorption/ionization imaging mass spectrometry in biological and clinical research. Chem. Rev. 2013, 113, 2309-2342.
5. Wu, C.; Dill, A. L.; Eberlin, L. S.; Cooks, R. G.; Ifa, D. R., Mass spectrometry imaging under ambient conditions. Mass Spectrom. Rev. 2013, 32, 218-243.
6. Laskin, J.; Lanekoff, I., Ambient Mass Spectrometry Imaging Using Direct Liquid Extraction Techniques. Anal. Chem. 2016, 88, 52-73.
7. Feider, C. L.; Krieger, A.; DeHoog, R. J.; Eberlin, L. S., Ambient ionization mass spectrometry: recent developments and applications. Anal. Chem. 2019, 91, 4266-4290.
8. Greer, T.; Sturm, R.; Li, L., Mass spectrometry imaging for drugs and metabolites. J Proteomics 2011, 74, 2617-2631.
9. Rao, W.; Pan, N.; Yang, Z., High resolution tissue imaging using the single-probe mass spectrometry under ambient conditions. J. Am. Soc. Mass Spectrom. 2015, 26, 986-993.
10. Nguyen, S. N.; Sontag, R. L.; Carson, J. P.; Corley, R. A.; Ansong, C.; Laskin, J., Towards high-resolution tissue imaging using nanospray desorption electrospray ionization mass spectrometry coupled to shear force microscopy. J. Am. Soc. Mass Spectrom. 2017, 29, 316-322.
11. Venter, A. R.; Douglass, K. A.; Shelley, J. T.; Hasman Jr, G.; Honarvar, E., Mechanisms of real-time, proximal sample processing during ambient ionization mass spectrometry. Anal. Chem. 2014, 86, 233-249.
12. Eberlin, L. S.; Ferreira, C. R.; Dill, A. L.; Ifa, D. R.; Cooks, R. G., Desorption electrospray ionization mass spectrometry for lipid characterization and biological tissue imaging. Biochim Biophys Acta Mol Cell Biol Lipids 2011, 1811, 946-960.
13. Wiseman, J. M.; Ifa, D. R.; Zhu, Y.; Kissinger, C. B.; Manicke, N. E.; Kissinger, P. T.; Cooks, R. G., Desorption electrospray ionization mass spectrometry: Imaging drugs and metabolites in tissues. Proc. Natl. Acad. Sci. U. S. A. 2008, 105, 18120-18125.
14. Campbell, D. I.; Ferreira, C. R.; Eberlin, L. S.; Cooks, R. G., Improved spatial resolution in the imaging of biological tissue using desorption electrospray ionization. Anal. Bioanal. Chem. 2012, 404, 389-398.
15. Laskin, J.; Heath, B. S.; Roach, P. J.; Cazares, L.; Semmes, O. J., Tissue imaging using nanospray desorption electrospray ionization mass spectrometry. Anal. Chem. 2012, 84, 141-148.
16. Yin, R.; Kyle, J.; Burnum-Johnson, K.; Bloodsworth, K. J.; Sussel, L.; Ansong, C.; Laskin, J., High spatial resolution imaging of mouse pancreatic islets using nanospray desorption electrospray ionization mass spectrometry. Anal. Chem. 2018, 90, 6548-6555.
17. Unsihuay, D.; Su, P.; Hu, H.; Qiu, J.; Kuang, S.; Li, Y.; Sun, X.; Dey, S. K.; Laskin, J., Imaging and analysis of isomeric unsaturated lipids through online photochemical derivatization of carbon–carbon double bonds. Angew. Chem. Int. Ed. 2021, 60, 7559-7563.
18. Van Berkel, G. J.; Kertesz, V.; Koeplinger, K. A.; Vavrek, M.; Kong, A. N. T., Liquid microjunction surface sampling probe electrospray mass spectrometry for detection of drugs and metabolites in thin tissue sections. J Mass Spectrom. 2008, 43, 500-508.
19. Van Berkel, G. J.; Kertesz, V.; King, R. C., High-throughput mode liquid microjunction surface sampling probe. Anal. Chem. 2009, 81, 7096-7101.
20. Swales, J. G.; Tucker, J. W.; Spreadborough, M. J.; Iverson, S. L.; Clench, M. R.; Webborn, P. J.; Goodwin, R. J., Mapping drug distribution in brain tissue using liquid extraction surface analysis mass spectrometry imaging. Anal. Chem. 2015, 87, 10146-10152.
21. Havlikova, J.; Randall, E. C.; Griffiths, R. L.; Swales, J. G.; Goodwin, R. J.; Bunch, J.; Styles, I. B.; Cooper, H. J., Quantitative imaging of proteins in tissue by stable isotope labeled mimetic liquid extraction surface analysis mass spectrometry. Anal. Chem. 2019, 91, 14198-14202.
22. Yin, R.; Burnum-Johnson, K. E.; Sun, X.; Dey, S. K.; Laskin, J., High spatial resolution imaging of biological tissues using nanospray desorption electrospray ionization mass spectrometry. Nat. Protoc. 2019, 14, 3445-3470.
23. Hale, O. J.; Cooper, H. J., Native Mass Spectrometry Imaging of Proteins and Protein Complexes by Nano-DESI. Anal. Chem. 2021, 93, 4619-4627.

24. Hale, O. J.; Hughes, J. W.; Cooper, H. J., Simultaneous spatial, conformational, and mass analysis of intact proteins and protein assemblies by nano-DESI travelling wave ion mobility mass spectrometry imaging. Int. J. Mass Spectrom. 2021, 116656.

25. Yan, X.; Zhao, X.; Zhou, Z.; McKay, A.; Brunet, A.; Zare, R. N., Cell-Type-Specific Metabolic Profiling Achieved by Combining Desorption Electrospray Ionization Mass Spectrometry Imaging and Immunofluorescence Staining. Anal. Chem. 2020, 92, 13281-13289.

26. Eberlin, L. S.; Liu, X.; Ferreira, C. R.; Santagata, S.; Agar, N. Y.; Cooks, R. G., Desorption electrospray ionization then MALDI mass spectrometry imaging of lipid and protein distributions in single tissue sections. Anal. Chem. 2011, 83, 8366-8371.

27. Huizing, L. R.; Ellis, S. R.; Beulen, B. W.; Barré, F. P.; Kwant, P. B.; Vreeken, R. J.; Heeren, R. M., Development and evaluation of matrix application techniques for high throughput mass spectrometry imaging of tissues in the clinic. Clin. Mass Spectrom. 2019, 12, 7-15.

28. Zavalin, A.; Yang, J.; Hayden, K.; Vestal, M.; Caprioli, R. M., Tissue protein imaging at 1 μm laser spot diameter for high spatial resolution and high imaging speed using transmission geometry MALDI TOF MS. Anal. Bioanal. Chem. 2015, 407, 2337-2342.

29. Ellis, S. R.; Cappell, J.; Potočnik, N. O.; Balluff, B.; Hamaide, J.; Van der Linden, A.; Heeren, R. M., More from less: high-throughput dual polarity lipid imaging of biological tissues. Analyst 2016, 141, 3832-3841.

30. Barré, F.; Rocha, B.; Dewez, F.; Towers, M.; Murray, P.; Claude, E.; Cillero-Pastor, B.; Heeren, R.; Siegel, T. P., Faster raster matrix-assisted laser desorption/ionization mass spectrometry imaging of lipids at high lateral resolution. Int. J. Mass Spectrom. 2019, 437, 38-48.

31. Bednarik, A.; Kuba, P.; Moskovets, E.; Tomalová, I.; Krásenský, P.; Houška, P.; Preisler, J., Rapid matrix-assisted laser desorption/ionization time-of-flight mass spectrometry imaging with scanning desorption laser beam. Anal. Chem. 2014, 86, 982-986.

32. Spraggins, J. M.; Caprioli, R. M., High-speed MALDI-TOF imaging mass spectrometry: rapid ion image acquisition and considerations for next generation instrumentation. J. Am. Soc. Mass Spectrom. 2011, 22, 1022-1031.

33. Prentice, B. M.; Chumbley, C. W.; Caprioli, R. M., High‐speed MALDI MS/MS imaging mass spectrometry using continuous raster sampling. J Mass Spectrom. 2015, 50, 703-710.

34. Tillner, J.; Wu, V.; Jones, E. A.; Pringle, S. D.; Karancsi, T.; Dannhorn, A.; Veselkov, K.; McKenzie, J. S.; Takats, Z., Faster, more reproducible DESI-MS for biological tissue imaging. J. Am. Soc. Mass Spectrom. 2017, 28, 2090-2098.

35. Unsihuay, D.; Qiu, J.; Swaroop, S.; Nagornov, K. O.; Kozhinov, A. N.; Tsybin, Y. O.; Kuang, S.; Laskin, J., Imaging of triglycerides in tissues using nanospray desorption electrospray ionization (Nano-DESI) mass spectrometry. Int. J. Mass Spectrom. 2020, 448, 116269.

36. Lanekoff, I.; Burnum-Johnson, K.; Thomas, M.; Cha, J.; Dey, S. K.; Yang, P.; Conaway, M. C. P.; Laskin, J., Three-dimensional imaging of lipids and metabolites in tissues by nanospray desorption electrospray ionization mass spectrometry. Anal. Bioanal. Chem. 2015, 407, 2063-2071.

37. Nguyen, S. N.; Liyu, A. V.; Chu, R. K.; Anderton, C. R.; Laskin, J., Constant-distance mode nanospray desorption electrospray ionization mass spectrometry imaging of biological samples with complex topography. Anal. Chem. 2017, 89, 1131-1137.

38. Li, X.; Yin, R.; Hu, H.; Li, Y.; Sun, X.; Dey, S. K.; Laskin, J., An integrated microfluidic probe for mass spectrometry imaging of biological samples. Angew. Chem. Int. Ed. 2020, 59, 22388-22391.

39. Stjernström, M.; Roeraade, J., Method for fabrication of microfluidic systems in glass. J. Micromech. Microeng. 1998, 8, 33.

40. Iliescu, C.; Taylor, H.; Avram, M.; Miao, J.; Franssila, S., A practical guide for the fabrication of microfluidic devices using glass and silicon. Biomicrofluidics 2012, 6, 016505.

41. Lanekoff, I.; Heath, B. S.; Liyu, A.; Thomas, M.; Carson, J. P.; Laskin, J., Automated platform for high-resolution tissue imaging using nanospray desorption electrospray ionization mass spectrometry. Anal. Chem. 2012, 84, 8351-8356.

42. Hu, H.; Yin, R.; Brown, H. M.; Laskin, J., Spatial Segmentation of Mass Spectrometry Imaging Data by Combining Multivariate Clustering and Univariate Thresholding. Anal. Chem. 2021, 93, 3477-3485.

43. Luxembourg, S. L.; Mize, T. H.; McDonnell, L. A.; Heeren, R. M., High-spatial resolution mass spectrometric imaging of peptide and protein distributions on a surface. Anal. Chem. 2004, 76, 5339-5344.

44. Patterson, N. H.; Tuck, M.; Van de Plas, R.; Caprioli, R. M., Advanced registration and analysis of MALDI imaging mass spectrometry measurements through autofluorescence microscopy. Anal. Chem. 2018, 90, 12395-12403.

45. Klein, S.; Staring, M.; Murphy, K.; Viergever, M. A.; Pluim, J. P., Elastix: a toolbox for intensity-based medical image registration. IEEE Trans. Med. Imaging 2009, 29, 196-205.

For Table of Contents Only